ACS APPLIED MATERIALS & INTERFACES

www.acsami.org

Research Article

Microstructured Reflective Coatings on Commodity Textiles for Passive Personal Cooling

Evan D. Patamia, Megan K. Yee, and Trisha L. Andrew*

Cite This: https://doi.org/10.1021/acsami.4c15984

Read Online

ACCESS | Metrics & More | Article Recommendations | Supporting Information

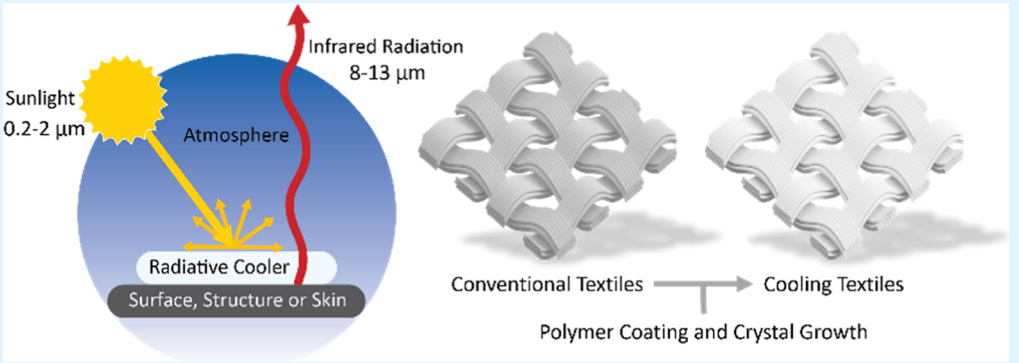

ABSTRACT: As the effects of climate change become more severe and widespread, maintaining personal thermal homeostasis becomes necessary for survival. In principle, advanced textiles and garments have the ability to leverage light absorption, transmission and/or reflection, in addition to straightforward convection, to heat or cool bodies in extreme temperature conditions. For cooling, in particular, surfaces adept at selectively reflecting or refracting high-energy incident light (200 nm−2.5 mm) from the sun while transmitting or emitting infrared light (8−13 mm) from radiant body heat boast the ability to maintain cooler body temperatures, even when exposed to direct sunlight and the open sky. Here, we present a strategy to transform common clothing into implements for passive personal cooling. As confirmed by Mie scattering calculations, cheap and biocompatible calcium carbonate and barium sulfate micro/nanoparticles are found to serve as suitable reflectors for radiative cooling. Finite-difference time domain simulations reveal, surprisingly, that higher reflectance is achieved with surface coatings containing these materials, as compared to extruded metamaterial fibers containing $CaCO_3$ and $BaSO_4$ particles embedded within a polymer matrix. A stepwise process involving photoinitiated chemical vapor deposition and ion-exchange driven crystal growth is used to create a lamellar composite coating comprised of alternating $CaCO_3$ and $BaSO_4$ nano/microparticle layers directly on the surface of common fabrics. A polyester poplin fabric coated in this manner shows a cooling ability of up to 8 °C compared to an uncoated sample, achieving a maximum cooling of 6 °C below ambient temperature. Wash and durability testing of the lamellar coating reveal no mechanical degradation and no evident attenuation in the material's performance, affirming its resilience and long-term effectiveness as a functional textile coating for personal cooling. We also assess the performance of our coated fabrics in multiple outdoor environments to conclude that we can achieve up to 3.4 °C of sub-ambient cooling in optically complex built environments.

KEYWORDS: *radiative cooling, coating, chemical vapor deposition, crystal growth, calcium carbonate*

1. INTRODUCTION

Steadily increasing average temperatures across the world threaten to render urban environments unlivable, outside of the careful enclosure of high-cost air-conditioned environments. In the past 10 years, over 15,000 added deaths in urban environments have been reported after heat wave events.[1] At current heating rates, with no reduction in fossil fuel consumption, the proportion of people worldwide who are exposed to deadly heatwaves for more than 20 days a year is expected to rise from its current level of 30% to almost 74%.[2] Climate simulations that take into account both temperature and humidity by using a quantity named the "wet-bulb temperature" project that parts of the Middle East, India, China, Africa, Central America, and Southeast Asia will all experience wet-bulb temperatures above 35 °C in the next 30 years,[3] past the threshold of human survivability.[4] This reality motivates the immediate need for effective, low cost, and low

Received: September 18, 2024
Revised: October 10, 2024
Accepted: October 15, 2024

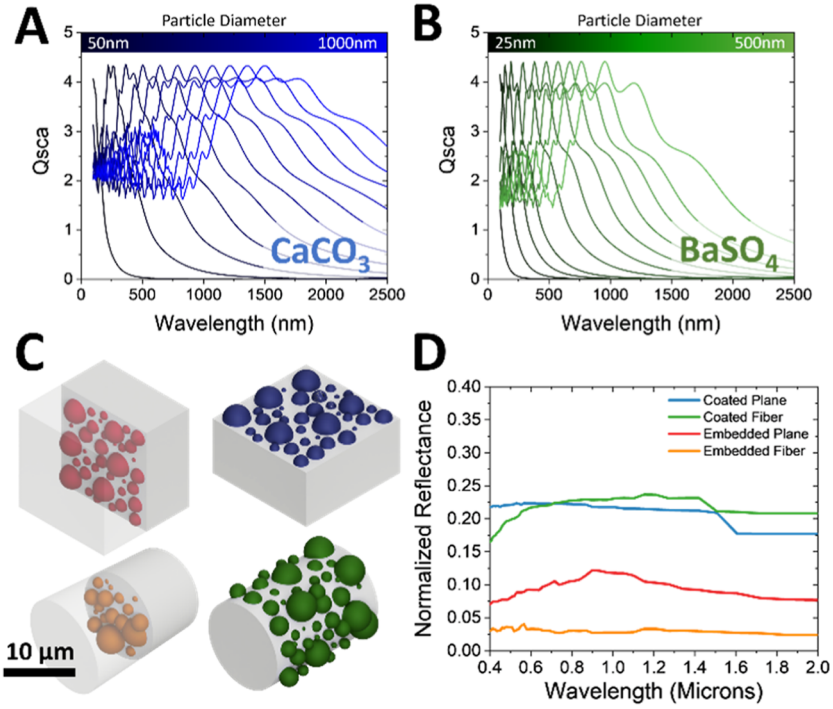

Figure 1. Results from simulation experiments. (A) Mie scattering results from distributed particle sizes of $CaCO_3$ in air (50−1000 nm). (B) Mie scattering results from distributed particle sizes of $BaSO_4$ in air (25−500 nm). (C) Illustrations of finite difference time domain (FDTD) models, showing PMMA matrix (gray) and colored $CaCO_3$ particles. The four evaluated architectures were: embedded plane (red), coated plane (blue), embedded fiber (orange) and coated fiber (green). (D) Comparative reflective contribution of particles in different architectures revealed by FDTD calculations. Reflectance values were normalized for volume of $CaCO_3$ in each architecture and the contribution from PMMA matrix was subtracted.

energy-consuming personal cooling that creates minimal inconvenience to individuals.

The main causes of personal overheating are direct exposure to incident sunlight from the sky and indirect exposure to reflected light from the ground and surrounding environment,[5,6] both of which are types of optical heating. One strategy to promote personal cooling is, therefore, to prevent or mitigate optical heating with the use of radiative coolers, which are composed of reflective and emissive materials.[7] Specifically for personal cooling, a radiative cooler should be 100% emissive in the atmospheric transmission window (ATW) from 8 to 13 μm and 100% reflective in the solar emission spectrum from 200 to 2500 nm.[8] In this way, a radiative cooler worn on the body can reflect incident ultraviolet−visible−infrared (UV−vis−NIR) light from the sun, limiting the (photo)thermal energy absorbed by the body, but still allow for free transmission of radiated body heat in the form of mid-infrared light through the radiative cooler, away from the body and into the external environment. Being a passive optical effect, such radiative cooling requires no additional energy input.[9]

Previous attempts to create wearable radiative coolers made use of specialty composite fibers,[10−13] fluorinated polymers,[14−17] porous polymer membranes,[18,19] engineered nanomaterials,[20,21] and/or noble metal coatings.[22,23] Although these iterations validated the concept of wearable radiative cooling, the use of expensive materials, heavy metals, environmentally harmful fluorinated polymers and/or complex fabrication methods rendered them impractical for high volume manufacturing and widespread adoption. Further, the performance of most wearable radiative cooling systems were mainly assessed under open-sky conditions with direct incident sunlight,[24,25] whereas their performance in comparatively challenging and optically complex built environments went unexamined.

Here we present a structured composite that can be applied as an ultrathin finish (i.e., coating) on any premade garment or commodity textile to transform existing clothing into radiative coolers. We discuss two key process advances—the use of a dry chemical vapor deposition process to create multiple conformal and interleaving polymer layers on the surface of any textile, and the direct seeding and growth of alternating $CaCO_3$ and $BaSO_4$ micro- and nanoparticles from these polymer surfaces—which, in sum, afford a robust lamellar coating that is highly reflective in the solar emission window but also allows common commodity fabrics to maintain their emissivity in the ATW. We also assess the cooling performance of coated fabrics in a selection of model optical environments to confirm that fabric-based radiative coolers are capable of providing cooling effects in complex urban settings.

2. RESULTS AND DISCUSSION

2.1. Design of a Radiative Cooling Coating. *2.1.1. Reflectors.* Several engineered nanomaterials, including aluminum oxide, titanium dioxide, hafnium oxide and noble metal micro/nanoparticles, have been previously used in radiative cooling systems for their ability to reflect as close to 100% of the solar spectrum as possible. In this work, we evaluated two metal salts whose applicability in wearable radiative coolers has not yet been demonstrated: calcium carbonate and barium sulfate. These salts were identified because of their low cost, wide availability, biocompatibility and putative near-infrared

https://doi.org/10.1021/acsami.4c15984
ACS Appl. Mater. Interfaces XXXX, XXX, XXX−XXX

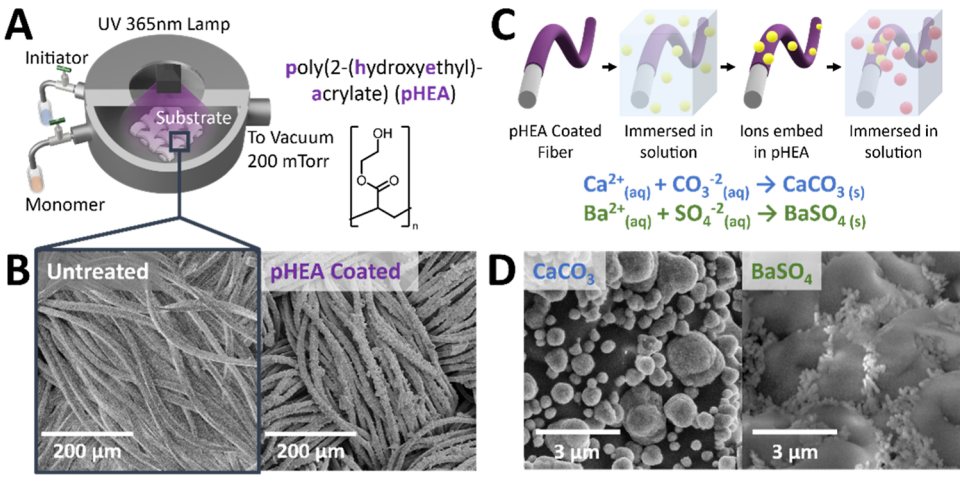

Figure 2. Summary of stepwise coating process. (A) Illustration of the piCVD reactor used to create polymer coatings and the structure of poly(2-(hydroxyethyl)-acrylate) (pHEA). (B) SEM images of a woven polyester poplin fabric before and after coating with pHEA using piCVD. (C) Illustration of the process for on-surface particle growth and reaction scheme for the formation of $CaCO_3$ and $BaSO_4$. (D) SEM Images of $CaCO_3$ (left) and $BaSO_4$ (right) particles grown on the surface of a pHEA treated polyester poplin fabric.

reflectance.[26−31] Before any experiments were conducted, we chose to run a series of simulations to evaluate the reflective performance of these two salts in varying form factors.

The reflectance of broad-spectrum incident sunlight by a material is best understood as a Mie scattering phenomenon. Therefore, utilizing open-source software,[32] Mie scattering profiles were calculated for both barium sulfate and calcium carbonate micro/nanoparticles, paying special attention to their scattering efficiency in the solar emission window between 200 nm and 2.5 μm. The Mie scattering efficiency (Q_{sca}), defined as the ratio of the simulated scattering cross section and the geometric cross section,[33] is plotted in Figure 1a,b for $CaCO_3$ and $BaSO_4$ particles with diameters between 50−1000 nm. The scattering efficiencies calculated for both $CaCO_3$ and $BaSO_4$ particles were comparable in magnitude to those predicted for alumina and titania nanoparticles over the solar emission range. As expected, instead of indiscriminate scattering, different sized particles preferentially interacted with specific wavelengths of incident light, and larger sized particles displayed scattering maxima at longer wavelengths. Overall, calcium carbonate particles displayed reasonable scattering efficiencies for wavelengths up to 2500 nm, whereas barium sulfate particles displayed a sharp drop in scattering efficiency for incident light past ca. 1500 nm, even at larger particle sizes. These results suggested that a polydisperse ensemble of salt particles that varied in both size and composition was necessary to achieve broadband scattering of incident light over the entire solar emission spectrum. Advantageously, our simulations also revealed that both $CaCO_3$ and $BaSO_4$ particles did not notably interact with light within the ATW (8−13 μm), meaning that inclusion of these reflectors would not attenuate the thermal emissivity of a radiative cooling device (Figure S1).

2.1.2. Optimal Spatial Distribution. In most prior iterations, reflective micro and nanoparticles were stochastically embedded within polymer films or fibers to create radiative coolers.[27−29,34] To quantify the effects of the spatial distribution of these embedded particles on reflectance, we executed FDTD calculations on representative models. Simulated reflectance data were generated and compared across the visible spectrum region from 400 to 2000 nm for representative $CaCO_3$ particles with a Gaussian size distribution between 50−1000 nm. These size-disperse particles were then embedded within or coated on a representative poly(methyl methacrylate) (PMMA) matrix, a common structural polymer that is also optically similar to the polyester and nylon fibers used in modern clothing. Four total architectures were evaluated: monofilament fibers (i.e., cylinders) with particles either embedded within the fiber bulk or restricted to the surface of the fibers as coatings; and two-dimensional membranes (i.e., flat planes) with either bulk embedded or surface coated particles (Figure 1c). The reflectance of the PMMA matrix was subtracted from all samples, and calculated reflectance spectra were normalized to the total volume of $CaCO_3$ particles present in each architecture to allow for accurate comparison. As shown in Figure 1d, at equivalent size dispersity and loading, surface-coated particles were up to ten times more reflective than their embedded counterparts in both fiber and membrane geometries. This was due to increased refraction at the $CaCO_3$−air interface as compared to the $CaCO_3$−PMMA interface, which increased the total intensity of light reflected back toward the source.

This result has immediate, broad-reaching implications for the design of radiative coolers. Most radiative coolers in the literature, textile or otherwise, either embed reflectors in a paintable matrix or place them inside extruded fibers, which, as our simulations suggest, should attenuate their optical performance. On the other hand, while surface coated particles exhibit optimal optical behavior in our simulations, in practice, micro/nanoparticle coated fibers and membranes are notoriously fragile and readily exhibit particle erosion and component leaching unless carefully attached to a surface. With these issues in mind, we set out to create an organic−inorganic composite coating containing covalently immobilized, polydisperse $CaCO_3$ and $BaSO_4$ particles situated at the outermost air interface.

2.2. Fabricating the Radiative Cooling Coating. *2.2.1. Crystal Growth on Fabric Surfaces.* Inspired by previous work to imitate the structure of nacre in mollusk shells, we devised a two-step process to grow micro/nanocrystals of $CaCO_3$ and $BaSO_4$ directly from the surface

https://doi.org/10.1021/acsami.4c15984
ACS Appl. Mater. Interfaces XXXX, XXX, XXX−XXX

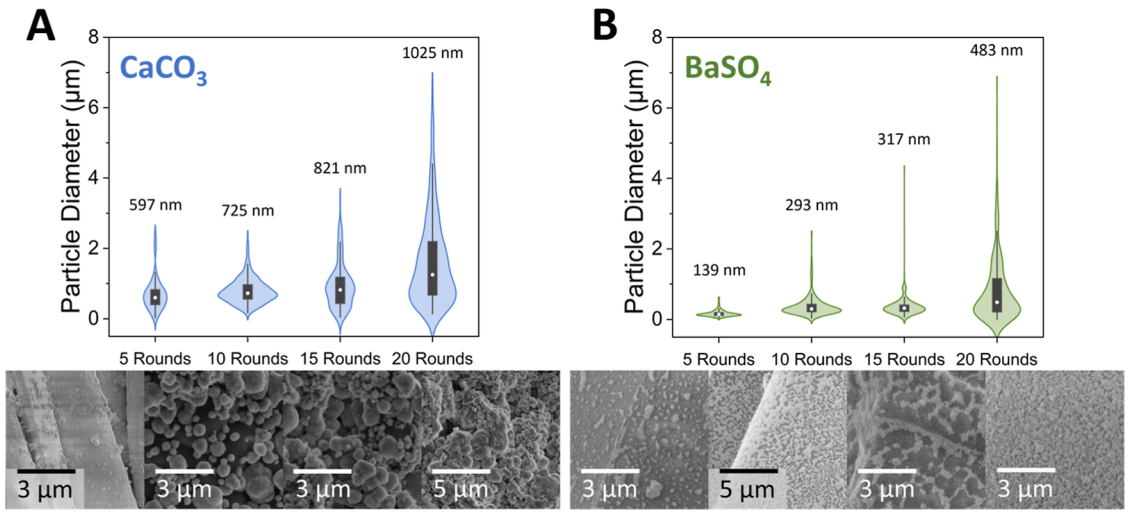

Figure 3. Particle size distribution plots for $CaCO_3$ (A) and $BaSO_4$ (B) particles grown on the surface of pHEA coated polyester poplin with corresponding SEM images for (left to right) 5,10,15, and 20 crystal growth cycles provided for each salt. Average particle sizes are reported at the top of each violin plot.

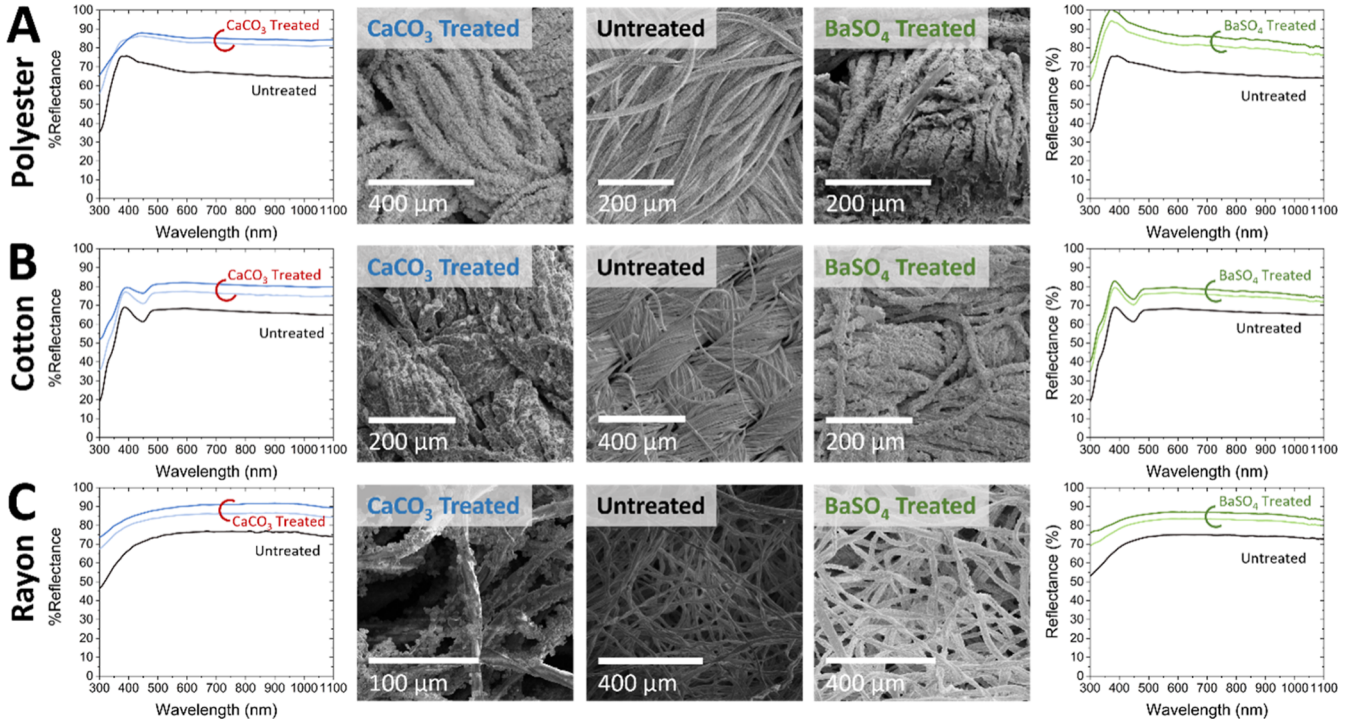

Figure 4. Optical properties of various coated fabrics. Wavelength-resolved reflectance spectra and SEM images of pHEA coated (A) polyester poplin, (B) cotton and (C) rayon fabrics subjected to ten (light) or 20 (dark) $CaCO_3$ (blue) or $BaSO_4$ (green) growth cycles.

of fabrics. Previously, Rubira et al. reported a method by which $CaCO_3$ crystals were grown directly on the surface of polyethylene sheets using a poly(acrylic acid) seed layer.[35] Although this seed layer could be easily spun coat onto flat, nonporous surfaces, its analogous application on common fabrics rendered them stiff, brittle and nonporous. Further, the poly(acrylic acid) textile coating was readily soluble in water and would likely wash away during laundering. In substitution, we elected to apply a hydrophilic coating of poly(2-(hydroxyethyl)-acrylate) (pHEA) using a previously reported photoinitiated chemical vapor deposition (piCVD) process (Figure 2).[36] A uniform and conformal coating of pHEA was created on diverse, off-the-shelf fabrics using piCVD, as confirmed by scanning electron microscopy (SEM) (Figure S2). The pHEA coating was formed as a ca. 10 μm thick cladding around each individual fiber component of all investigated fabrics, with no observable instances of fiber-to-fiber bridging or pore filling over the entire 5 × 5 in. coated area. The pHEA coating was not perceptible to touch and, therefore, did not observably modify the handfeel of the fabrics investigated. Due to the dual hydrogen bond-donating and Lewis basic nature of the pendant hydroxyl moiety found in the repeat unit structure of pHEA, we posited that the pHEA coating would covalently bind calcium and barium cations[37] and, therefore, serve as a bonding and seed layer for $CaCO_3$ and $BaSO_4$ micro/nanocrystals.

https://doi.org/10.1021/acsami.4c15984
ACS Appl. Mater. Interfaces XXXX, XXX, XXX−XXX

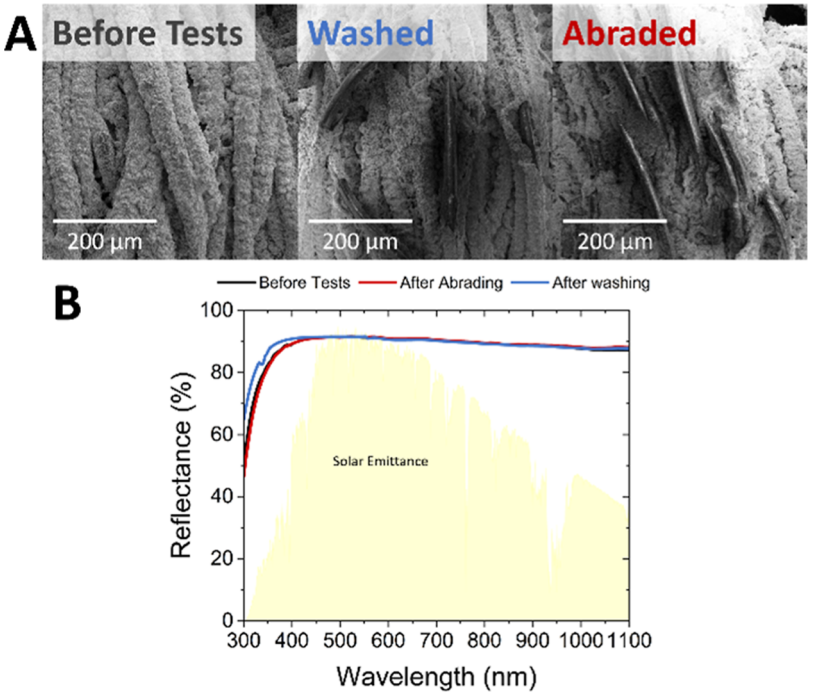

Figure 5. Washing and abrasion test results. (A) SEM images showing minimal coating erosion or damage after washing and mechanical abrasion. (B) Wavelength-resolved reflectance spectra of coated polyester poplin before and after testing.

To grow $CaCO_3$ and $BaSO_4$ microcrystals directly from the surface of pHEA coated fabrics, samples were sequentially immersed in a series of dilute solutions containing Ca^{2+} and $(CO_3)^{2-}$ ions, and/or Ba^{2+} and $(SO_4)^{2-}$ ions, with clean-solvent rinsing steps in-between to remove physisorbed and weakly adsorbed ions or aggregates (Figure S3). Growth of $CaCO_3$ microcrystals proceeded both vertically (i.e., normal to the surface) and laterally along the surface of the polymer layer, despite variances in the underlying morphology of the pHEA coating (Figure S4). Samples were imaged using SEM after 5,10,15, and 20 such crystal growth cycles. At least three different locations within each 5 × 5 in. sample were imaged at constant magnification. Particle and/or crystal sizes in each image were then quantified using an image analysis program. As shown in Figure 3, clear increases in average particle size could be effected by increasing the number of immersion cycles, for both $CaCO_3$ and $BaSO_4$. Additionally, the size distribution spanned small nanometer scale particles to larger, micron scale crystals. As revealed by the Mie scattering simulations discussed earlier, this distribution of sizes was ideal for reflecting broad spectrum incident light. Notably, similar control over particle size and surface coverage could not be achieved when off-the-shelf fabrics were directly subjected to crystal growth without a pHEA coating (Figure S5). Further, any crystals that formed on the surface of uncoated fabrics were often rubbed away during handling or eroded away with clean-solvent washes.

2.2.2. Fabric Scope and Optical Characterization. This method of fabric modification and crystal growth was not limited to a particular fiber material or weave type. To show the wide scope of this method, several off-the-shelf fabrics were coated, and their reflectance and transmittance properties measured using a diffuse reflectance spectrometer (Figure 4). Three fabrics were chosen to represent a wide variety of fiber compositions and weave patterns: cotton muslin, polyester poplin and rayon felt were chosen to represent natural and synthetic fabrics, and a nonwoven fabric, respectively. The piCVD process created an equivalently uniform and conformal pHEA coating in all cases, with no evident difference in surface uniformity or coating morphology between natural and synthetic fibers and woven/nonwoven samples. The subsequent seeded crystal growth process also proceeded comparably for all tested fabrics and resulted in comparable particle size dispersity, similar to the polyester poplin discussed earlier. All tested fabrics also displayed similar optical characteristics upon being coated with the either a pHEA $CaCO_3$ or pHEA-$BaSO_4$ coating: the reflectance of all coated fabrics between 300−1100 nm increased, while their average transmittance decreased, as expected upon adding an optically reflective coating.

2.2.3. Breathability and Washability. Compliant with standardized protocol provided by the American Association of Textile Chemists and Colorists (AATCC), a series of washing and wear tests were conducted to evaluate the longevity and ruggedness of our coating (AATCC LP1). Transmittance and reflectance spectra of all fabrics, as well as SEM images, were taken before and after these treatments. No substantial difference in the optical properties of the fabrics were observed before and after all such testing (Figure 5). While small abrasions were sometimes noted on the bias grain of woven fabrics after abrasion tests, such defects were expected and, importantly, did not observably change the optical properties of coated fabrics.

Breathability tests were conducted using the ASTM E96 desiccant method. Coated fabrics displayed near-identical vapor permeance to their untreated counterparts, meaning that the coating had no effect on the breathability of the starting fabric (Figure S6).

2.3. Optimized Fabric-Based Radiative Cooler. *2.3.1. Coating Composition.* Using the stepwise coating process described above, we optimized the coating composition to achieve maximal subambient cooling under direct

https://doi.org/10.1021/acsami.4c15984
ACS Appl. Mater. Interfaces XXXX, XXX, XXX−XXX

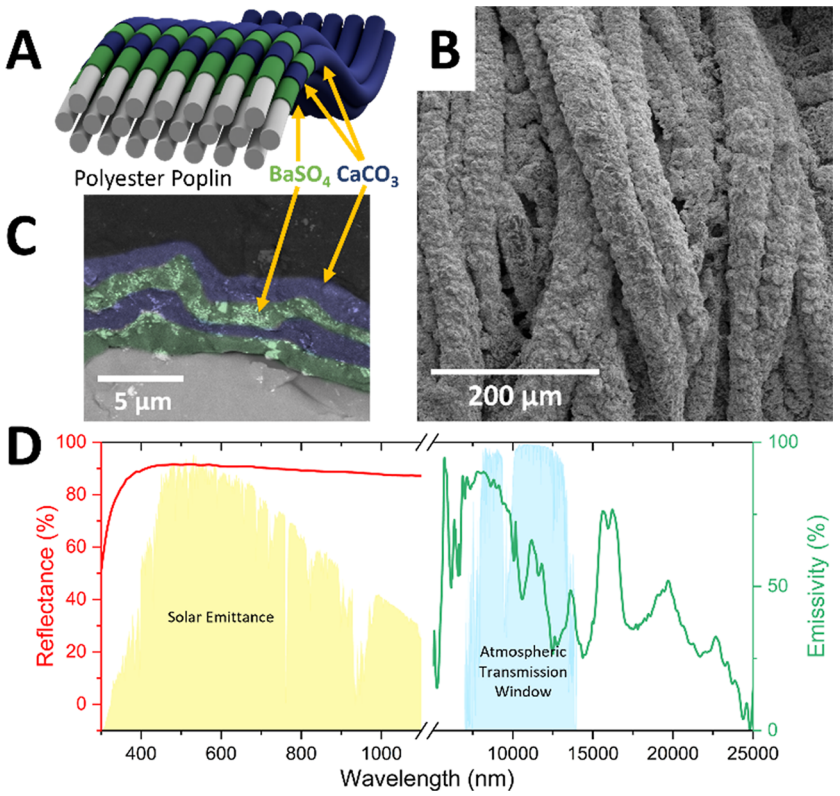

Figure 6. (A) Illustration of the optimized four-layer lamellar composite coating on woven polyester poplin. (B) SEM image of the outermost surface of a polyester poplin fabric coated with the four-layer lamellar composite. (C) False color cross-sectional SEM image revealing the discrete $CaCO_3$ and $BaSO_4$ lamellae of the coating. (D) Wavelength-resolved reflectance and emission spectra of the coated fabric, with the ASTM G173-03 solar emittance spectrum (yellow) and ATW (blue) highlighted.

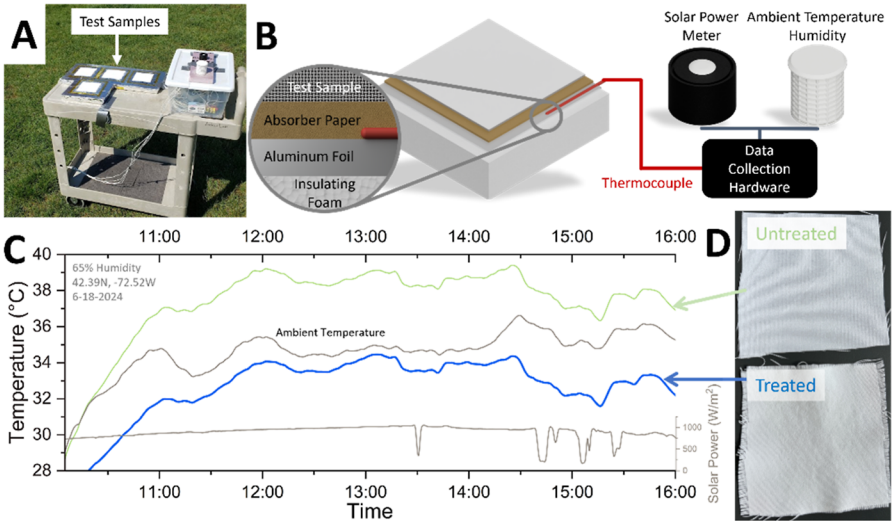

Figure 7. Outdoor test setup to evaluate radiative cooling. (A) Picture of the test setup with samples oriented horizontally (i.e., parallel to the ground) in an open field. (B) Illustration of the test platform showing thermocouple location, solar power meter, Stevenson screen, and data collection hardware. (C) Temperature profiles recorded by the test setup during peak solar hours. The surface under the coated fabric was, on average, 2.1 °C colder than ambient temperature (max: 6 °C, min: 0.5 °C). (D) Optical micrograph of untreated polyester poplin (top) and polyester poplin coated with a four-layer lamellar composite (bottom).

exposure to sunlight. Focusing on polyester poplin fabrics due to their prevalence in familiar garments, we initially evaluated the radiative cooling performance of samples coated with either the pHEA-$CaCO_3$ or the pHEA-$BaSO_4$ composite material described earlier. While both coatings similarly enhanced the reflectance of polyester poplin in the solar emission window, sub-ambient cooling was, nonetheless, not evident.

To further improve the overall reflectance of the coating and, therefore, enable a cooling effect, we leveraged the unique ability of the piCVD process to create discrete microscale lamellae of alternating reflectors. Unlike solution coating

https://doi.org/10.1021/acsami.4c15984
ACS Appl. Mater. Interfaces XXXX, XXX, XXX−XXX

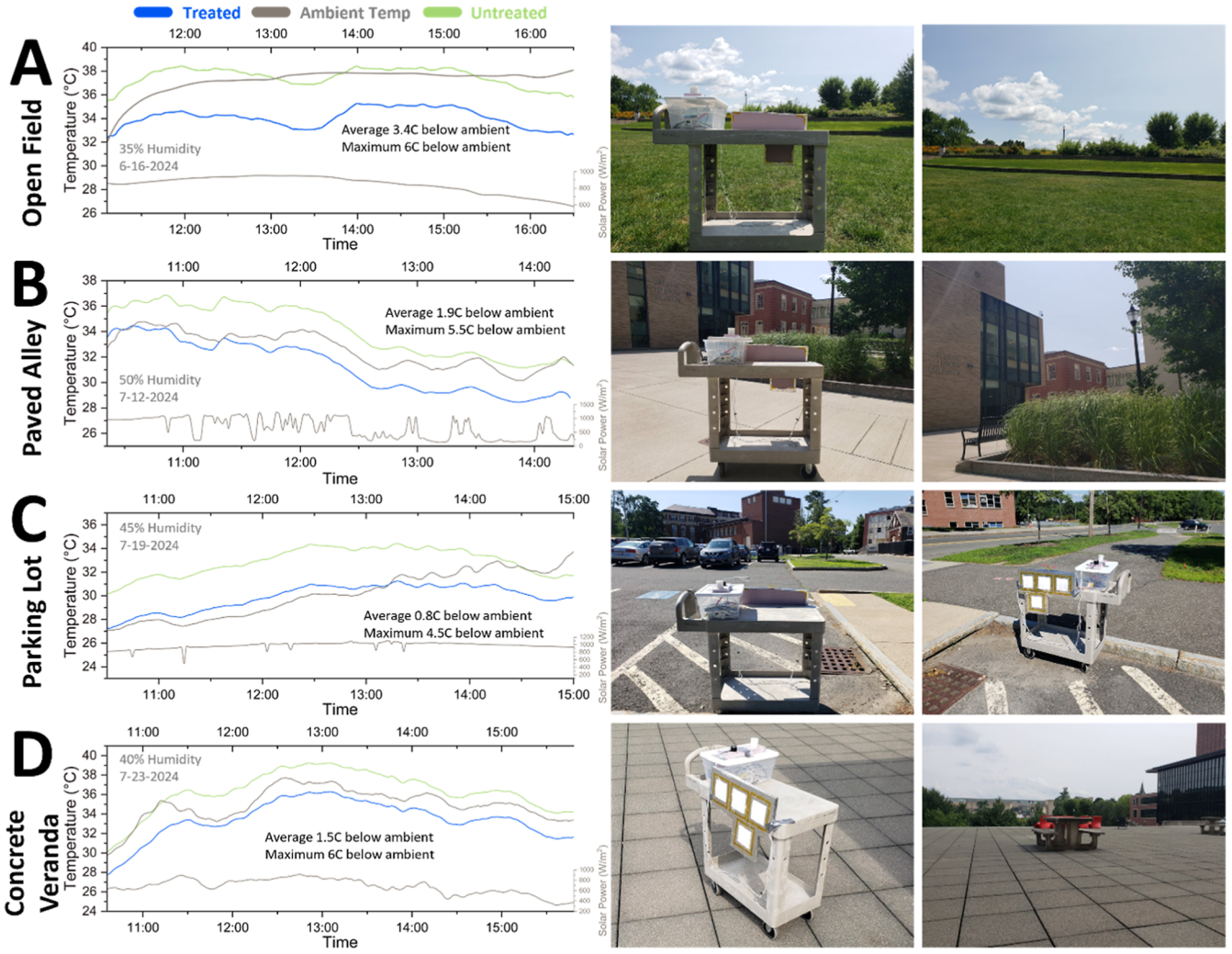

Figure 8. Outdoor evaluation in representative urban settings. Temperature profiles recorded by the test setup with samples oriented vertically (i.e., perpendicular to the ground) are shown on the left, accompanied by pictures of the corresponding testing environment on the right. (A) Open grass field (open sky). (B) Concrete-paved alley between three multistory buildings (obscured sky). (C) Car-filled, asphalt-paved parking lot surrounded by multistory buildings. (D) Concrete veranda.

methods that can dissolve or intermix with carefully formed underlayers, piCVD, being a dry process, allowed for bottom-up growth of multiple polymer−particle layers. Inspired by dielectric mirrors, we fabricated a four-layer coating composed of alternating $CaCO_3$ and $BaSO_4$ particles grown on interleaving pHEA layers (Figure 6). We hypothesized that such alternating material interfaces would increase scattering events and encourage interference, like in a dielectric mirror, to ultimately afford greater reflectance across the solar emission spectrum. Images of the lamellar four-layer coating on polyester poplin are shown in Figure 6, with a false-color cross-section SEM image of an isolated polyester poplin fiber delineating each radial lamella in Figure 6c. We note that, consistent with the suggestions provided by our FDTD calculations, this optimized coating contained exposed $CaCO_3$ particles situated at the outermost air interface to allow for optimal Mie scattering from this exterior surface. While the other three particle layers were buried within the coating, in an ostensibly disadvantageous arrangement, we posited that the presence of discrete and alternating pHEA-$CaCO_3$ and pHEA-$BaSO_4$ radial lamellae introduced refractive index mismatched interfaces that would encourage additional refraction, even if buried. Indeed, a polyester poplin fabric treated with this four-layer coating displayed the highest reflectance in the solar window among all investigated samples, while also maintaining the high thermal emissivity observed for untreated poplin in the ATW (Figure S7). As expected, the four-layer coating also decreased the intensity of bleed-through UV−vis light that was transmitted through the porous fabric from an average of 31% for uncoated polyester poplin to only 6% for coated samples (Figure S8).

2.3.2. Outdoor Evaluation. The cooling properties of this optimized coated fabric were evaluated using a custom-built test bed, which consisted of an insulating foam board wrapped in aluminum foil and covered by a colored spacer paper (Figure 7). Test samples were then placed on this spacer paper with the coating facing outward. The colored spacer paper represented the body or a similarly absorptive surface that would be optically heated by any light transmitted through the test sample. A thermocouple was attached to this spacer paper to log the temperature of the absorber (i.e., body). The insulated foam test bed ensured that this spacer paper was thermally isolated during outdoor tests and, therefore, could only be heated by incident light reaching its surface. Reflective

https://doi.org/10.1021/acsami.4c15984
ACS Appl. Mater. Interfaces XXXX, XXX, XXX−XXX

aluminum foil prevented the surface of the foam board from being optically heated by transmitted sunlight. To maintain the same volume of still air space between each test sample and the spacer paper and enable accurate comparison between different data sets, all test samples were shielded from air flow between layers by taping their four edges to the foam test bed. During each outdoor test, at least three samples of equivalent size were simultaneously evaluated: a coated fabric and its uncoated counterpart, and a bare spacer paper lacking any fabric covering. In this fashion, each outdoor test allowed direct simultaneous comparison of the temperatures experienced by a body exposed to incident sunlight, a regularly clothed body exposed to the same intensity of solar radiation and a body covered with our coated fabrics.

Outdoor tests were first conducted with samples placed parallel to the ground, with the four-layer coating directly facing the open sky (Figure 7a). The data presented here was collected over June and July 2024 in Amherst, Massachusetts, during multiple hot, cloudless days with varying levels of humidity (between 35 and 50% relative humidity). The temperature underneath treated and off-the-shelf fabrics were logged simultaneously, in addition to the ambient temperature, humidity and incident solar power. As seen in Figure 7c, polyester fabrics treated with our four-layer lamellar coating allowed a surface to remain up to 8 °C cooler than a surface covered with an untreated off-the-shelf counterpart.

Next, we performed evaluations in varied urban environments with the test bed aligned vertically, at a 90° angle to the ground (Figure 8). In this orientation, since test samples did not exclusively face the sky, optical heating could be caused by any combination of direct and (diffuse) reflected solar radiation and ground/surface radiated heat (i.e., mid-infrared light). Such a vertical sample placement more accurately simulated the scenario in which a clothed body is being optically heated by the environment. This vertical orientation also subjected samples to a more strenuous optical load, as multi-angular, incoherent beams of light over a large wavelength range needed to be rejected to effect notable sub-ambient cooling. As these tests were conducted in the northern hemisphere, samples were always oriented facing SSW (225°) to maximize the intensity of solar radiation incident on their surface over a 12 h period. Four representative environments were explored: an open grass field, a car-filled and asphalt-paved parking lot, an open concrete seating area, and an enclosed urban alleyway with obscured sky access.

Despite large variations in incident solar radiation and external humidity across different testing days, our coated fabric afforded between an average of 0.8 to 3.4 °C of sub-ambient cooling in all built environments. Notably, in the parking lot test case (Figure 8c), a polyester poplin fabric coated with our four-layer composite material allowed a surface to remain 3.6 °C colder than a surface covered with regular polyester poplin, and 0.8 °C colder than the external temperature. This observation has significant implications for pedestrian and cyclizt health in asphalt-rich built environments, which experience inordinately large instances of heat-stress related deaths and injuries.[38]

We attribute the ability of our coated fabrics to effect subambient cooling in multiple environments to the optical advantages conferred by our conformal lamellar coating. Because it contains refractive index-mismatched lamellae and multiple scattering interfaces, our optimized four-layer coating maintains notable reflectance at multiple angles of incidence (Figure S9). Upon being applied conformally onto the topographically complex surface of a woven fabric, this structured coating can then interact with an even broader angular range of incident light, thus allowing our coated fabrics to reject diffuse reflected solar radiation and ground/surface radiated heat.

3. CONCLUSIONS

Here we present a composite material that can be applied as a coating on any premade garment or commodity textile to transform existing clothing into radiative coolers. Through Mie scattering and FDTD simulations we elucidate the optimal size ranges and positioning of $CaCO_3$ and $BaSO_4$ particles to enhance reflection of solar radiation. Then, we leverage two key processes—polymer chemical vapor deposition, and direct seeding and on-surface growth of $CaCO_3$ and $BaSO_4$ particles—to realize a conformal and lamellar composite coating on poplin fabrics that allows underlying surfaces to remain up to 8 °C cooler when exposed to direct sunlight than uncoated fabric counterparts. Using AATCC compliant test protocol, we confirm that our coated fabrics are durable to washing and wearing, and exhibit unaltered breathability and handfeel as compared to uncoated counterparts. We also assess the performance of our coated fabrics in multiple outdoor environments to conclude that we can achieve up to 3.4 °C of sub-ambient cooling in optically complex built environments.

4. MATERIALS AND METHODS

4.1. Materials. Hydroxymethylpropiophenone (HMPP), (2-hydroxyethyl)-acrylate (HEA), calcium carbonate, calcium chloride, barium chloride, sodium carbonate, and sodium sulfate were purchased from Sigma-Aldrich at 99% purity. Methanol was purchased from Fisher scientific. Polyester, cotton and rayon felt fabric samples were purchased from an online retailer, onlinefabric-store.com.

4.2. Mie Scattering Simulations. Mie scattering simulations were conducted using open source software Pymie. Complex refractive index data for $CaCO_3$, and PMMA were collected from the public domain database refractiveindex.info.[39] A single-value refractive index for $BaSO_4$ was used (1.636 at 589 nm)[40] Simulations for $CaCO_3$ nanoparticles in air were run on particle size ranges from 50 to 1000 nm, $BaSO_4$ nanoparticles in air particle size ranges 25 to 500 nm.

4.3. FDTD Simulations. FDTD Simulations were run using Ansys Lumerical. A simulation time of 1000 fs and temperature of 300 K were chosen. Simulation spans were 20 × 20 × 20 μm with a minimum mesh step of 0.00025 μm. For plane simulations periodic boundary conditions were used for the x and y directions, for fiber simulations periodic conditions were only used in the x direction (on-axis with the fiber) all others were PML. A single plane wave source from 400 to 2000 nm was used. Complex refractive index data for $CaCO_3$, and PMMA were collected from the public domain database refractiveindex.info; the database was last accessed on August 28, 2024.[4] Reflectance magnitudes from each simulation scenario were normalized to the volume of microparticle present in the simulation, and the contribution of the PMMA matrix subtracted.

4.4. piCVD of pHEA. Inside a round vacuum chamber (250 mmø × 50 mm) a 5 × 5 in. fabric sample was placed and a rotary vacuum pump and LN2 Vapor Trap were used to apply a vacuum of 200 mTorr. Into a 10 mL glass ampule, 0.1 g HMPP and 1.0 g HEA was added and mixed, then the ampule was attached to a heated inlet line (110 °C) through a needle valve. Then a 365 nm UV LED (Darkbeam SK 68) was placed on top of a quartz glass window, filling the chamber with UV light. After this, the needle valve was opened 1/eighth of a full turn from the closed position. After 1 min, the needle

https://doi.org/10.1021/acsami.4c15984
ACS Appl. Mater. Interfaces XXXX, XXX, XXX−XXX

valve was opened completely. After the desired deposition time (typically 10 min) the UV source was turned off, and the needle valve closed, and the LN2 Vapor trap recharged with liquid nitrogen. Heating tape was removed from the vial and the chamber allowed to pump off any residual or unreacted monomer and initiator vapor for 5 min. Then the chamber could be opened to the atmosphere and the sample removed.

4.5. Crystal Growth. Samples for crystal growth were first prepared by a piCVD deposition of pHEA. Into four separate 500 mL crystallization dishes were added 250 mL of deionized (DI) water, methanol, and either solutions of 0.2 M $CaCl_2$ and 0.2 M $NaCO_3$, or solutions of 0.2 M $BaCl_2$ and 0.2 M $NaSO_4$. The crystal growth protocol followed this sequence: first, the sample was placed in a cation bath for 30 s; next, the sample was washed in the DI water bath for 30 s and the methanol bath for 10 s; then the sample was placed into the anion bath for 30 s; and, finally the sample was washed in the DI bath for 30 s and the methanol bath for 10 s (Figure S3). Subsequent rounds of crystal growth were conducted following these outlined steps.

4.6. Material Characterization. SEM images of fabrics were collected on an FEI Magellan 400 using beam settings of 3 kV and 50 pA. UV−vis Diffuse spectroscopy measurements were taken using a Thermo Scientific Evolution 220 with an ISA-220 integrating sphere accessory. Emissivity was measured using a Thermo Scientific Nicolet IS50 FTIR spectrometer with a Praying Mantis diffuse reflectance attachment, samples were measured against a KBr background.

4.7. Textile Tests. The AATCC LP1 protocol guidelines were followed to conduct wash and wear tests. Briefly, the wash test consisted of a 30 min agitated submergence in 10% laundry detergent solution with 300 rpm stirring. To gauge the mechanical durability of the coating, a 1 kg weight was placed on top of the treated fabrics with an untreated fabric acting as the abrader, then a simple pulling operation was executed at least 20 times, allowing the abrader to rub over the surface of the treated fabric. Transmittance and reflectance spectra of all fabrics, as well as SEM images, were taken before and after all individual tests.

Breathability tests were conducted using the ASTM E96 desiccant method. Inside several capped vials an equal mass of dried desiccant was placed. Identical holes 15 mm in diameter were drilled into the cap, and fabric samples were placed in between the cap and the vial and the exterior of the vial sealed with parafilm. Samples were then loaded into a sealed container alongside a humidity sensor and an open beaker of water. The weight of the desiccants was tracked over the course of 7 days, and permeance calculated.

4.8. Optimized Coating Process. A 5 × 5 in. sample of a white polyester poplin fabric was coated in pHEA via piCVD then treated to 20 Rounds of BaSO4 crystal growth. The next layer consisted of another pHEA deposition, and then 20 rounds of CaCO3 crystal growth. These two layers were then repeated, forming a 4 layer device.

4.9. Outdoor Testing. A custom test platform made of insulated polystyrene foam wrapped in a layer of aluminum foil was used to limit contribution to measured temperatures from the test stand. K-type thermocouples (PerfectPrime TL0400) were laid out on the test platform and centered on sample locations (5inx5in) and connected to a thermal datalogger (PerfectPrime TC0520). Then, a neutral-colored spacer paper (Pantone 16-0945, 0.2 mm thick) was placed on top of the thermocouples to act as a thermal absorber for transmitted light through the fabric. Solar power (Lutron SPM-1116SD) and ambient temperature and humidity were collected using a Stevenson screen shield. Vertical testing of the samples was conducted by setting the samples at a 85° angle to the ground, with the panel pointing southwest (225° N). Outdoor tests were run during varied weather conditions from 6 to 12−24 to 8−12−24 on-campus at UMASS Amherst in a variety of urban areas, and an open field (42°23′27″N 72°31′37″W).

■ ASSOCIATED CONTENT

Supporting Information

The Supporting Information is available free of charge at https://pubs.acs.org/doi/10.1021/acsami.4c15984.

Optical characterization and scanning electron microscope images (PDF)

■ AUTHOR INFORMATION

Corresponding Author

Trisha L. Andrew − *Department of Chemistry, University of Massachusetts Amherst, Amherst, Massachusetts 01003, United States; Department of Chemical Engineering, University of Massachusetts Amherst, Amherst, Massachusetts 01003, United States;* orcid.org/0000-0002-8193-2912; Email: tandrew@umass.edu

Authors

Evan D. Patamia − *Department of Chemistry, University of Massachusetts Amherst, Amherst, Massachusetts 01003, United States;* orcid.org/0000-0001-9052-8850

Megan K. Yee − *Department of Chemistry, University of Massachusetts Amherst, Amherst, Massachusetts 01003, United States*

Complete contact information is available at: https://pubs.acs.org/10.1021/acsami.4c15984

Author Contributions

The manuscript was written through contributions of all authors. All authors have given approval to the final version of the manuscript.

Funding

This work was supported by an Interdisciplinary Research Grant from the College of Natural Sciences at the University of Massachusetts Amherst.

Notes

The authors declare no competing financial interest.

■ REFERENCES

(1) Zou, J.; Lu, H.; Shu, C.; Ji, L.; Gaur, A.; Wang, L. Multiscale numerical assessment of urban overheating under climate projections: A review. *Urban Clim* **2023**, *49*, 101551.

(2) Mora, C.; Dousset, B.; Caldwell, I. R.; Powell, F. E.; Geronimo, R. C.; Bielecki, C. R.; Counsell, C. W. W.; Dietrich, B. S.; Johnston, E. T.; Louis, L. V.; et al. Global risk of deadly heat. *Nat. Clim. Chang.* **2017**, *7*, 501−506.

(3) Newth, D.; Gunasekera, D. Projected Changes in Wet-Bulb Globe Temperature under Alternative Climate Scenarios. *Atmosphere* **2018**, *9*, 187.

(4) Vecellio, D. J.; Wolf, S. T.; Cottle, R. M.; Kenney, W. L. Evaluating the 35°C wet-bulb temperature adaptability threshold for young, healthy subjects (PSU HEAT Project). *J. Appl. Physiol.* **2022**, *132*, 340−345.

(5) Zhao, H.; Wang, S.; Zhang, Y.; Zhao, L.; Zhai, Y.; Brown, R. D.; Jin, L.; Wu, R. The effect of solar radiation on pedestrian thermal comfort: A climate chamber experiment. *Build. Environ.* **2023**, *245*, 110869.

(6) Suhaimi, M. F. B.; Kim, W. G.; Cho, C.-W.; Lee, H. Impact of solar radiation on human comfort in a vehicle cabin: An analysis of body segment mean radiant temperature. *Build. Environ.* **2023**, *245*, 110849.

(7) Ren, S.; Han, M.; Fang, J. Personal Cooling Garments: A Review. *Polymers* **2022**, *14*, 5522.

(8) Catalanotti, S.; Cuomo, V.; Piro, G.; Ruggi, D.; Silvestrini, V.; Troise, G. The radiative cooling of selective surfaces. *Sol. Energy* **1975**, *17*, 83−89.
(9) Chen, M.; Pang, D.; Chen, X.; Yan, H.; Yang, Y. Passive daytime radiative cooling: Fundamentals, material designs, and applications. *EcoMat* **2022**, *4*, No. e12153.
(10) Zeng, S.; Pian, S.; Su, M.; Wang, Z.; Wu, M.; Liu, X.; Chen, M.; Xiang, Y.; Wu, J.; Zhang, M.; et al. Hierarchical-morphology metafabric for scalable passive daytime radiative cooling. *Science* **2021**, *373*, 692−696.
(11) Song, Y.-N.; Ma, R.-J.; Xu, L.; Huang, H.-D.; Yan, D.-X.; Xu, J.-Z.; Zhong, G.-J.; Lei, J.; Li, Z.-M. Wearable Polyethylene/Polyamide Composite Fabric for Passive Human Body Cooling. *ACS Appl. Mater. Interfaces* **2018**, *10*, 41637−41644.
(12) Peng, Y.; Chen, J.; Song, A. Y.; Catrysse, P. B.; Hsu, P.-C.; Cai, L.; Liu, B.; Zhu, Y.; Zhou, G.; Wu, D. S.; et al. Nanoporous polyethylene microfibres for large-scale radiative cooling fabric. *Nat. Sustain* **2018**, *1*, 105−112.
(13) Hsu, P.-C.; Song, A. Y.; Catrysse, P. B.; Liu, C.; Peng, Y.; Xie, J.; Fan, S.; Cui, Y. Radiative human body cooling by nanoporous polyethylene textile. *Science* **2016**, *353*, 1019−1023.
(14) Shi, M.; Song, Z.; Ni, J.; Du, X.; Cao, Y.; Yang, Y.; Wang, W.; Wang, J. Dual-Mode Porous Polymeric Films with Coral-like Hierarchical Structure for All-Day Radiative Cooling and Heating. *ACS Nano* **2023**, *17*, 2029−2038.
(15) Mandal, J.; Fu, Y.; Overvig, A. C.; Jia, M.; Sun, K.; Shi, N. N.; Zhou, H.; Xiao, X.; Yu, N.; Yang, Y. Hierarchically porous polymer coatings for highly efficient passive daytime radiative cooling. *Science* **2018**, *362*, 315−319.
(16) Sun, Y.; Ji, Y.; Javed, M.; Li, X.; Fan, Z.; Wang, Y.; Cai, Z.; Xu, B. Preparation of Passive Daytime Cooling Fabric with the Synergistic Effect of Radiative Cooling and Evaporative Cooling. *Adv. Mater. Technologies* **2022**, *7*, 2100803.
(17) Huang, M.-C.; Xue, C.-H.; Huang, J.; Liu, B.-Y.; Guo, X.-J.; Bai, Z.-X.; Wei, R.-X.; Wang, H.-D.; Du, M.-M.; Jia, S.-T.; et al. A hierarchically structured self-cleaning energy-free polymer film for daytime radiative cooling. *Chem. Eng. J.* **2022**, *442*, 136239.
(18) Zhang, Y.; Zhu, W.; Zhang, C.; Peoples, J.; Li, X.; Felicelli, A. L.; Shan, X.; Warsinger, D. M.; Borca-Tasciuc, T.; Ruan, X.; et al. Atmospheric Water Harvesting by Large-Scale Radiative Cooling Cellulose-Based Fabric. *Nano Lett.* **2022**, *22*, 2618−2626.
(19) Cai, L.; Song, A. Y.; Li, W.; Hsu, P.; Lin, D.; Catrysse, P. B.; Liu, Y.; Peng, Y.; Chen, J.; Wang, H.; et al. Spectrally Selective Nanocomposite Textile for Outdoor Personal Cooling. *Adv. Mater.* **2018**, *30*, 1802152.
(20) Lu, Y.; Chen, Z.; Ai, L.; Zhang, X.; Zhang, J.; Li, J.; Wang, W.; Tan, R.; Dai, N.; Song, W. A Universal Route to Realize Radiative Cooling and Light Management in Photovoltaic Modules. *Sol. RRL* **2017**, *1*, 1700084.
(21) Rehman, A.; Houshyar, S.; Mirabedini, A.; Michielsen, S.; Wang, X. Immobilization of nanodiamonds onto cotton fabric through polyurethane nanofibrous coatings for summer clothing. *Polym. Adv. Technol.* **2024**, *35*, No. e6222.
(22) Wu, R.; Sui, C.; Chen, T.-H.; Zhou, Z.; Li, Q.; Yan, G.; Han, Y.; Liang, J.; Hung, P.-J.; Luo, E.; et al. Spectrally engineered textile for radiative cooling against urban heat islands. *Science* **2024**, *384*, 1203−1212.
(23) Zou, C.; Ren, G.; Hossain, M. M.; Nirantar, S.; Withayachumnankul, W.; Ahmed, T.; Bhaskaran, M.; Sriram, S.; Gu, M.; Fumeaux, C. Metal-Loaded Dielectric Resonator Metasurfaces for Radiative Cooling. *Adv. Opt. Mater.* **2017**, *5*, 1700460.
(24) Kousis, I.; Pisello, A. L. Toward the Scaling up of Daytime Radiative Coolers: A Review. *Adv. Opt. Mater.* **2023**, *11*, 2300123.
(25) Huang, M.-C.; Yang, M.; Guo, X.-J.; Xue, C.-H.; Wang, H.-D.; Ma, C.-Q.; Bai, Z.; Zhou, X.; Wang, Z.; Liu, B.-Y.; et al. Scalable multifunctional radiative cooling materials. *Prog. Mater. Sci.* **2023**, *137*, 101144.
(26) Dong, Y.; Han, H.; Wang, F.; Zhang, Y.; Cheng, Z.; Shi, X.; Yan, Y. A low-cost sustainable coating: Improving passive daytime radiative cooling performance using the spectral band complementarity method. *Renew Energ* **2022**, *192*, 606−616.
(27) Li, X.; Peoples, J.; Huang, Z.; Zhao, Z.; Qiu, J.; Ruan, X. Full Daytime Sub-ambient Radiative Cooling in Commercial-like Paints with High Figure of Merit. *Cell Reports Phys. Sci.* **2020**, *1*, 100221.
(28) Li, X.; Peoples, J.; Yao, P.; Ruan, X. Ultrawhite BaSO4 Paints and Films for Remarkable Daytime Subambient Radiative Cooling. *ACS Appl. Mater. Interfaces* **2021**, *13*, 21733−21739.
(29) Lim, H.; Chae, D.; Son, S.; Ha, J.; Lee, H. CaCO3 micro particle-based radiative cooling device without metal reflector for entire day. *Mater. Today Commun.* **2022**, *32*, 103990.
(30) Tong, Z.; Peoples, J.; Li, X.; Yang, X.; Bao, H.; Ruan, X. Electronic and phononic origins of BaSO4 as an ultra-efficient radiative cooling paint pigment. *Mater. Today Phys.* **2022**, *24*, 100658.
(31) Sun, H.; Chen, Y.; Zeng, W.; Tang, F.; Bi, Y.; Lu, Q.; Mondal, A. K.; Huang, L.; Chen, L.; Li, J. Solution-processable, robust and sustainable cooler via nano-structured engineering. *Carbohydr. Polym.* **2023**, *314*, 120948.
(32) Ma, D.; Tuersun, P.; Cheng, L.; Zheng, Y.; Abulaiti, R. PyMieLab_V1.0: A software for calculating the light scattering and absorption of spherical particles. *Heliyon* **2022**, *8*, No. e11469.
(33) Nieto-Vesperinas, M. Fundamentals of Mie scattering. In *Dielectric Metamaterials*; Elsevier, 2020; pp 39−72..
(34) Zhang, X.; Cheng, Z.; Yang, D.; Dong, Y.; Shi, X.; Liang, H.; Wang, F.; Han, H.; Meng, W.; Shuai, Y.; et al. Scalable Bio-Skin-Inspired Radiative Cooling Metafabric for Breaking Trade-Off between Optical Properties and Application Requirements. *ACS Photonics* **2023**, *10*, 1624−1632.
(35) Silva, R.; Pereira, G. M.; Muniz, E. C.; Rubira, A. F. Calcium Carbonate Crystallization on a Polyethylene Surface Containing Ultrathin Layers of Hydrophilic Polymers. *Cryst. Growth Des.* **2009**, *9*, 3307−3312.
(36) Patamia, E. D.; Andrew, T. L. Photoinitiated chemical vapor deposition (piCVD) of composition tunable, ionically conductive hydrogels on diverse substrates. *Flex. Print. Electron.* **2023**, *8*, 045003.
(37) Ossola, F.; Tomasin, P.; Zorzi, C. D.; Habra, N. E.; Chiurato, M.; Favaro, M. New calcium alkoxides for consolidation of carbonate rocks. Influence of precursors' characteristics on morphology, crystalline phase and consolidation effects. *N. J. Chem.* **2012**, *36*, 2618−2624.
(38) Onishi, A.; Cao, X.; Ito, T.; Shi, F.; Imura, H. Evaluating the potential for urban heat-island mitigation by greening parking lots. *Urban For. Urban Green.* **2010**, *9*, 323−332.
(39) Polyanskiy, M. N. Refractiveindex.info database of optical constants. *Sci. Data* **2024**, *11*, 94.
(40) Lide, D. R. *CRC Handbook of Chemistry and Physics 88th Edition*; CRC Press, Taylor & Francis: Boca Raton, FL, 2007.

https://doi.org/10.1021/acsami.4c15984
ACS Appl. Mater. Interfaces XXXX, XXX, XXX−XXX